ACS OMEGA

Open Access

http://pubs.acs.org/journal/acsodf

Article

Enhanced Antibacterial Activity at Ag−Cu Nanojunctions: Unveiling the Mechanism with Simple Surfaces of CuNPs-on-Ag Films

Weerapat Li,[⊥] Supphanat Anantachaisophon,[⊥] Thanakrit Vachiraanun,[⊥] Worachon Promchaisri,[⊥] Pongpop Sangsawang,[⊥] Pattarapon Tanalikhit, Somlak Ittisanronnachai, Thassanant Atithep, Passapan Sanguanchua, Arjaree Ratanasangsathien, Mathus Jirapunyawong, Siriporn Suntiworapong, Sakol Warintaraporn,* and Yutichai Mueanngern*

Cite This: *ACS Omega* 2023, 8, 34919−34927

Read Online

ACCESS | Metrics & More | Article Recommendations | Supporting Information

ABSTRACT: Deposition of CuNPs on silver film gives rise to the formation of active Ag−Cu interfaces leading to dramatic enhancements in antibacterial activity against *Escherichia coli*. Transmission electron microscopy (TEM) and energy-dispersive X-ray spectroscopy (EDAX) analyses reveal that CuNPs are covered in a thin Cu_2O shell, while X-ray photoelectron spectroscopy measurements (XPS) reveal that the Ag film samples contain significant amounts of Ag_2O. XPS analyses show that the deposition of CuNPs on Ag films leads to the formation of a photoactive Ag_2O-Cu_2O heterostructure. Following a *Z*-scheme mechanism, electrons from the conduction band of Ag_2O recombine with photogenerated holes from the valence band of Cu_2O. Consequently, electrons at Cu_2O's conduction band render Cu reduced and cause reductive activation of surface oxygen species on Cu forming reactive oxygen species (ROS). Interaction between metallic Cu and ROS species leads to the formation of a $Cu(OH)_2$ phase. Both ROS and $Cu(OH)_2$ species have previously been reported to lead to enhanced antibacterial properties. Holes on Ag_2O produce a highly oxidized AgO phase, a phase reported to exhibit excellent antibacterial properties. Quantitative analysis of Cu and Ag high-resolution X-ray photoelectron spectroscopy (HR-XPS) spectra directly reveals several-fold increases in these active phases in full agreement with the observed increase in antibacterial activities. This study provides insight and surface design parameters by elucidating the important roles of Ag and Cu's bifunctionality as active antibacterial materials.

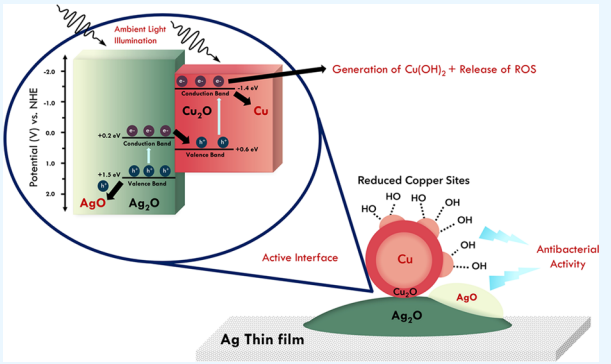

INTRODUCTION

Antibacterial surfaces have garnered much interest in recent years, particularly during the COVID-19 pandemic.[1−4] Metal nanoparticles are commonly used in antibacterial surfaces due to their high surface area/size ratio allowing for intimate contact with bacterial cell walls.[5,6] Mechanisms behind these antibacterial surfaces range from the formation of reactive oxygen species (ROS) catalyzed by metal surfaces, as well as the release of metal ions resulting in the disruption of ATP production as well as cell wall impairment.[7,8] Ag and Cu metal nanoparticles are commonly used for such applications.[8−13] In addition to their small penetrable size and oxidative tendency, dissociated ions of both Ag and Cu also exhibit strong affinities toward the thiol groups present on cell walls. This suggests another potential antibacterial mechanism: the interaction of copper and silver ions with the thiol groups found in proteins, which are crucial for enzymatic activity, leading to the inactivation of enzymes. It has been reported that heavy metals react with proteins by combining with thiol groups, which leads to the inactivation of the proteins.[14−16] Although the mechanism detailed above is generally accepted in the scientific community, a comprehensive understanding of the driving force behind the release of these ions, which may stem from a combination of structural and electronic properties intrinsic to each metal, remains elusive.[17,18] In addition, different types of metal phases have also been reported to exhibit very high antibacterial activity. Reports from Clavier et al. and Karkhanechi et al. indicate that $Cu(OH)_2$ can also act as a highly active antibacterial phase, although claimed origins of this observed effect vary widely from increased Cu ion release to release of surface OH radicals from Cu sites.[19,20]

Several studies have reported strong interactions across two metal phases leading to enhanced catalytic and antibacterial activity.[21−23] Peridakaki et al. reported significantly increased

Received: June 16, 2023
Accepted: August 31, 2023
Published: September 14, 2023

antibacterial activity when Ag/Cu hybrid structures on graphene oxide supports were evaluated against *Escherichia coli* (*E. coli*). This was attributed to structural interactions between the Ag and the Cu phases.[24] In studies conducted by Hans et al., inductively coupled plasma mass spectrometry (ICP-MS) data reveals a markedly higher release of Cu ions when Ag−Cu alloys are used as antibacterial surfaces as compared to monometallic systems of Ag and Cu alone.[25] Another study by Bankier et al. suggested that the synergistic effect between Cu and Ag arises from Cu's ability to perforate holes in bacterial cell membranes, allowing for Ag to efficiently enter the cell—subsequently damaging cell interior and sabotaging cell division.[21] Other types of synergistic effects have also been observed, including those that stem from metal/metal oxide and metal-oxide/metal-oxide systems.[26−28] On metal−metal oxide systems, core−shell nanoparticles of Ag@Cu_2O have been reported to lead to the formation of a heterostructure at the interface of the two materials allowing for efficient electron−hole pair separation.[29] Density functional theory (DFT) calculations by Feng et al. have shown that photoinduced charge transfer can occur when the Fermi energy of Ag lies close to the conduction band minimum of Cu_2O, leading to increased antibacterial activity.[30] Study on metal oxide/metal oxide system of Ag_2O−Cu_2O heterostructure by Guleria et al. also reports enhanced performance in dye degradation reactions arising from the formation of reactive hydroxyl and oxygen radicals—which can also have drastic effects on antibacterial activities.[31] Even though these studies provide strong evidence that the amplified antibacterial activity is due to strong interactions between Ag and Cu, no surface spectroscopic study has been carried out on simple colloid-thin film model surfaces in order to investigate the origins of these effects.

Recent advances in nanofabrication, colloid synthesis, and lithography have allowed for the fabrication of well-controlled planar surfaces. The ability to control morphological parameters at the nanoscale has led to the widespread use of planar surface systems in studying different types of surface chemical phenomena. These so-called "model surfaces" can be systematically controlled to affect different catalytic and/or antibacterial trends.[32−35] These trends can be used to complement existing proposed mechanisms and bridge the gap between experimental observables and computational results. Effects arising from the bifunctionality of two materials are known as strong metal−support interactions (SMSI), usually induced by strong bonding interactions between two different material phases. These interactions can be induced by alloying or exposing two materials to reactive gases at elevated temperatures. However, several reports have demonstrated that mere deposition of colloidal structures on thin film supports can lead to robust bonding interactions, resulting in changes to material activity.[36−39] To further investigate the effects of the Ag−Cu interface, we synthesized the Cu nanoparticles (CuNPs) via a robust-simple method and deposited the particles via drop-casting on electron-beam Ag silver thin films and tested the samples against *E. coli*. Gram-negative *E. coli* strains were chosen due to their thinner cell walls, which would allow for better interaction with the antibacterial surfaces. As CuNPs utilized in the majority of antibacterial applications are often inconsistent in structural morphologies, we decided to adjust the amount of PVP accordingly to emulate the structural characteristics of these nanoparticles while maintaining uniform particle size distributions.[40] We show that the presence of newly formed Ag−Cu interfaces leads to significant enhancement in antibacterial activity relative to Cu and Ag controls. X-ray photoelectron spectroscopy (XPS) studies reveal that Cu exists as Cu_2O prior to deposition on Ag film substrates forming Cu_2O−Ag_2O interfaces. Upon contact with Ag, the Cu 2p spectra begin to exhibit a much stronger metallic character, whereas Ag 3d becomes noticeably more oxidized. The antibacterial mechanisms can be explained by a charge transfer process from the conduction band of Ag_2O, under visible light illumination, to Cu_2O, which in turn reduces metal surface sites at the Cu phase and diminishes oxygen species near the metal surface forming ROS which are reported to be highly antibacterial. The origins of the observed surface $Cu(OH)_2$ phase, as detected via XPS measurements, could be attributed to reactions of these ROS species with metallic copper. Additionally, the charge transfer process from Ag_2O to Cu_2O generates a highly oxidized AgO phase, which has been shown in previous studies to have excellent antibacterial properties. We propose that Cu, $Cu(OH)_2$, and AgO are the active phases and the formation of these phases is due to a charge transfer process between the interface of the two materials.

METHODS

Surface Preparation. *Silver Thin Film Deposition.* Silver films were deposited onto a silicon wafer substrate via thermal evaporation deposition using a Kurt J. Lesker system, operating at a deposition rate of 0.5−0.8 nm/s at a base pressure of 5.0×10^{-5} torr. The silver film was deposited at a thickness of 100 nm, the deposition rate was monitored using a quartz crystal microbalance. Individual samples, approximately 0.5 cm × 0.5 cm in size, were diced with a diamond head to obtain suitable samples for Cu deposition.

CuNPs and Cu_2O Nanocubes Synthesis.[40] CuNPs were synthesized by following a previously reported protocol with slight modification. Solutions of poly(vinylpyrrolidone) (PVP) (0.30 M, 3 mL) in anhydrous ethylene glycol (EG), $CuSO_4 \cdot 5H_2O$ (0.10 M, 3 mL) in EG, and ascorbic acid (0.25 M, 3 mL) in EG were prepared. The PVP solution was stirred with a magnetic stirrer and was heated to 140 °C in two-neck round-bottom flasks. Solutions of $CuSO_4 \cdot 5H_2O$ and ascorbic acid were injected simultaneously, dropwise, into the hot PVP solution at a rate of approx. 0.25 mL/min. The solution was heated and stirred for an hour. Once the solution turned reddish-brown, it was cooled to 80 °C and allowed to age for approx. 1 h. The reaction system was cooled to room temperature, then it was diluted with ethanol and centrifuged (2000 rpm, 15 min) six times. The nanoparticles were deposited by directly drop-casting the solution in ethanol on 0.5 cm × 0.5 cm Ag film samples.

Cu_2O nanocubes were synthesized by mixing 0.0576 g of sodium dodecyl sulfate and 8410 μL of 0.1 M $CuSO_4$ with continuous stirring. After 5 min, 40 μL of a 1 M NaOH solution and 1450 μL of a 0.2 M sodium ascorbate solution were added, and the solution was left to stir for 10 min. The final product was centrifuged at 12,000 rpm and purified by water/ethanol wash steps.[41]

CuNPs Deposition on Silver Thin Film. CuNPs were drop-cast onto the silver thin films. The process was done by pipetting 7.78 $\mu L/mm^2$ of CuNP suspension onto a silver thin film. The silver thin film was then dried under ambient conditions for 1 h. The process is repeated for 3 samples to obtain statistically significant measurements. The process was

https://doi.org/10.1021/acsomega.3c04303
ACS Omega 2023, 8, 34919−34927

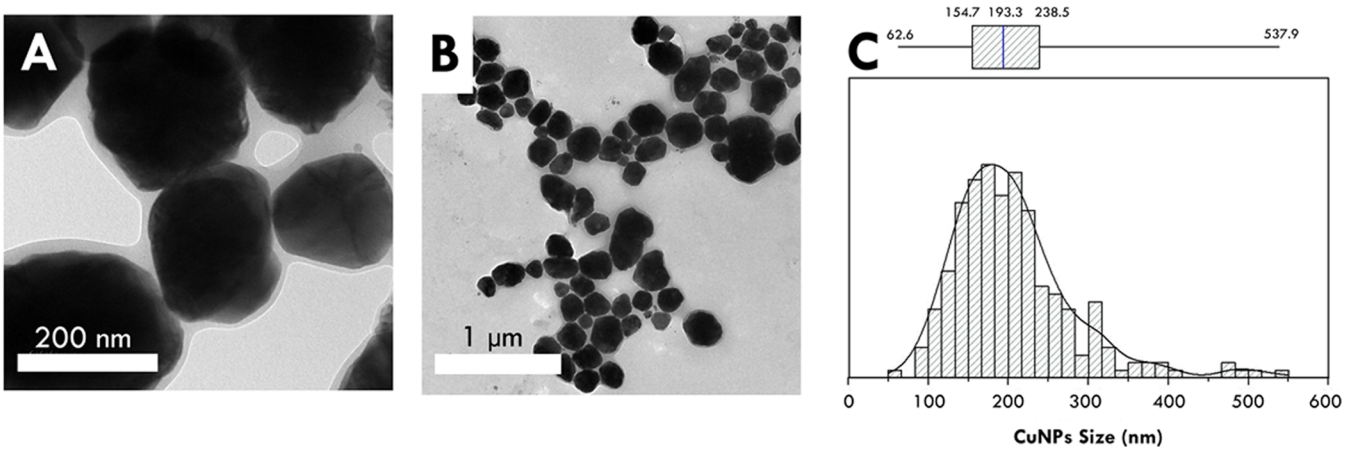

Figure 1. (A, B) TEM images of colloidal CuNPs. (C) Quantified size distribution of synthesized CuNPs, around 206 nm.

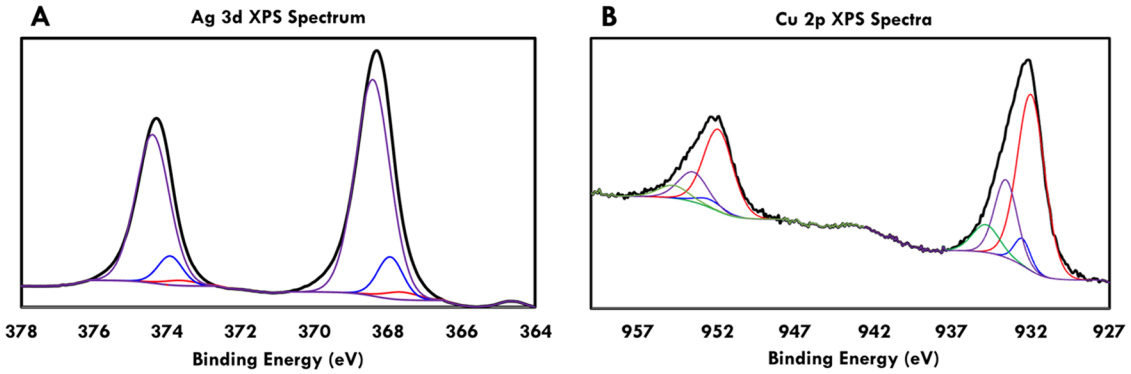

Figure 2. (A) Ag 3d HR-XPS spectra of 100 nm electron-beam-deposited Ag film. Features at 367.65, 367.95, and 368.30 eV corresponding to AgO, Ag_2O, and Ag, respectively. (B) HR-XPS spectrum of Cu 2p. Features at 932.0, 932.5, 933.59, and 934.88 eV corresponding to Cu_2O, Cu metal, CuO, and $Cu(OH)_x$, respectively.

replicated on a 300-mesh copper grid to characterize the surface coverage of the CuNPs on Ag film samples.

Antibacterial Activity Assessment.[42] The antibacterial efficiency of the film samples was assessed using *E. coli*. This assessment involved measuring the optical density (OD) at 620 nm of the bacteria solution and comparing it with control experiments—these were reference experiments conducted without any samples in the bacterial medium, and others conducted without any bacterial medium. Agar media for *E. coli* was prepared using the appropriate composition in an Erlenmeyer flask. Once all of the necessary equipment was autoclaved, the prepared media was poured into a Petri dish and left to solidify for 1.5 h. Using an inoculating loop, the bacterial solution was transferred from the stock to the agar media. The dish was incubated for 24 h to allow for bacteria to proliferate. After 24 h, colonies of bacteria were observed. A colony was then selected from the dish and transferred into a prepared Luria-Bertani broth. The solution was subsequently mixed with a vortex mixer. Using a pipette, the solution was transferred into the sterile 96-well plate with 200 μL pipetted into each well for OD 620 measurement. A control solution, which was broth without bacteria, was also added to serve as a reference for antibacterial activity analysis. The film samples—CuNPs on a silicon wafer, blank silver thin film, and CuNPs on silver thin film of various percentages of coverage—were put into the specified wells. The 96-well plate was incubated at 37 °C and subjected to an orbital shake at 150 rpm for 24 h. During incubation, the plate was removed twice, at 12 and 18 h, for OD 620 measurement of each well using the Microplate Reader (Halo LED 96). It should be noted that the films were removed from the wells prior to each measurement to prevent interference with the OD 620 value of the solution. The films were then placed back after the measurement.

Characterization. Various characterization techniques were utilized to analyze the prepared samples and ascertain their properties.

AFM Imaging. The surface roughness of the prepared silver thin film was determined using an atomic force microscope (AFM) (Park NX10).

TEM and EDAX Imaging. Bright-field high-resolution transmission electron microscopy (TEM) images and energy-dispersive X-ray spectroscopy (EDAX) plots were collected using a JEOL-ARM300F TEM microscope with an accelerating voltage of 200 kV. The morphology and surface coverage of the nanoparticles, which had been drop-cast on the 300-mesh copper TEM grids, were characterized through these means. Samples were degassed in a pumping station for 30 min prior to analysis.

XPS Surface Analysis. XPS measurements were performed using a ULVAC-PHI 5000 Versa Probe II, equipped with a micro-focused Mg Kα X-ray source (1253.6 eV). The probe operated at 25 W (with a voltage of 15 kV) and featured a hemispherical analyzer with a multichannel detector. The base pressure for the operation was at 10^{-10} mbar. Atomic fractions are retrieved from peak area fitting of Ag 3d and Cu 2p normalized to relative sensitivity factors.

https://doi.org/10.1021/acsomega.3c04303
ACS Omega 2023, 8, 34919−34927

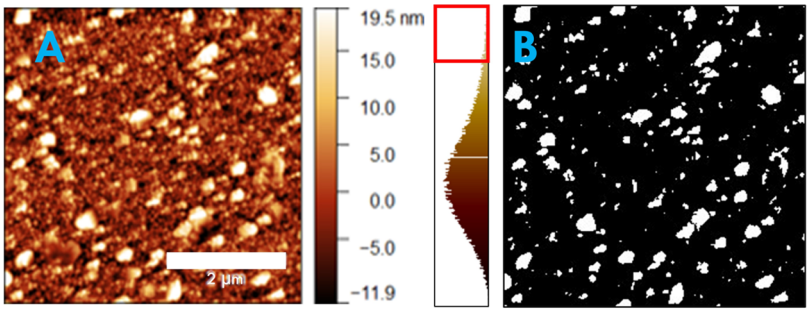

Figure 3. (A) Atomic force microscopy (AFM) image of the Ag film showing the surface topology. (B) Defects on the surface of Ag film calculated from ImageJ software, along with the histogram on the left depicting the area distribution of each surface height and the threshold set for the height of surface defects (highlighted in red box).

Image Analysis. Images retrieved from both TEM and AFM instruments were analyzed using ImageJ software. Through this analysis, the size distribution of CuNPs and the coverage of oxide surfaces were determined, respectively.

RESULTS AND DISCUSSION

Characterization of Ag and Cu. CuNPs were synthesized and deposited on Ag thin films. Figure 1A shows the TEM characterization of synthesized colloidal CuNPs. CuNP size distribution was calculated from Figure S1. As depicted in Figure 1B, the synthesized CuNPs have a diameter of 200 nm. XPS characterization was performed on CuNPs and Ag film samples to elucidate the surface states of the two phases prior to the formation of active Ag−Cu interfaces.

Figure 2A shows the high-resolution X-ray photoelectron spectroscopy (HR-XPS) spectra of Ag 3d. Features at 367.65, 367.95, and 368.30 eV correspond to AgO, Ag_2O, and Ag phases, respectively.[43] It is clear from Figure 2A that the surface of Ag consists mainly of Ag followed by Ag^+ (Ag_2O). Previous XPS studies on thermally evaporated Ag thin films have also reported similar surface compositions. Figure 2B shows HR-XPS spectra of Cu 2p, with a dominant feature at 932.0 eV corresponding to Cu_2O observed followed by 932.5, 933.59, and 934.88 eV corresponding to Cu, CuO, and $Cu(OH)_2$, respectively.[43] Results from Figure 2 indicate the presence of two important phases: Ag_2O and Cu_2O.

AFM characterization of Ag film indicates an rms roughness of 6.754 nm, as depicted in Figure 3A. Ag nanofilm roughness is in agreement with the reported AFM characterization of Ag thin films prepared via thermal evaporation. Based on previous AFM studies, which have shown that the coalescence of grains on thin film metal surfaces is indicative of oxide defects, this information was utilized to calculate the composition of the silver oxide islands on the silver film samples.[44] Figure S2 and Table S1 indicate that surface defects account for 10.23% of the entire plot. Although this does not prove that these grains are in fact Ag_2O, it is interesting to note that the percentage of oxide defects correlates with the surface concentration of silver(I) oxide quantified from Ag XPS spectra analysis. The presence of an Ag_2O can be detrimental in the formation of a heterostructure with other metal oxide materials.

The nature of the Cu_2O was further investigated using EDAX mapping on CuNPs. Figure 4A reveals a thin oxide shell covering the structure of the CuNPs. Further analysis along different profiles of the nanoparticles is shown in Figure 4B and Table S2 in the Supporting Information, which reveals a

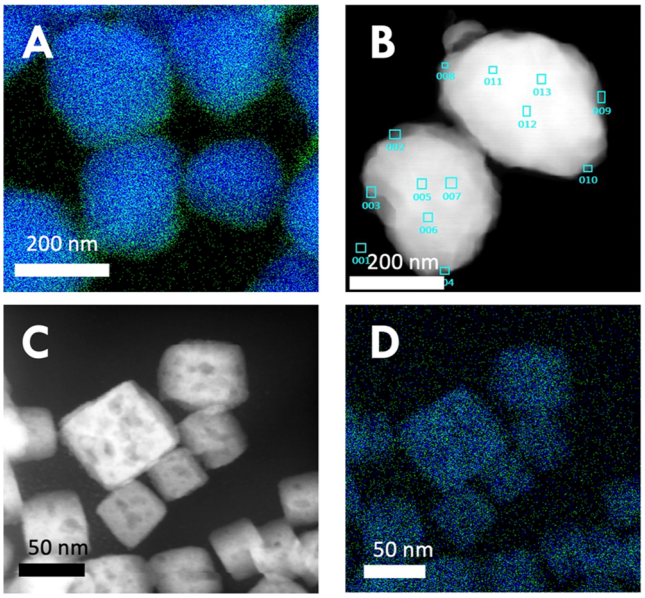

Figure 4. (A) EDAX mapping of oxygen and copper on CuNP, where green represents O regions and blue represents Cu regions. (B) HAADF image of two isolated CuNPs: EDAX analysis at the shell reveals a Cu/O ratio of 80, 20%, while analysis through the center of the nanoparticle reveals a 99−100% Cu content. (C, D) HAADF and EDAX mapping of separately synthesized Cu_2O nanoparticles.

Cu content of 70% and an O of 30% localized on the nanoparticle shell on analysis spots 4, 9, and 10 (see Supporting Information Table S2 corresponding to values for each spot). It is interesting to note that this corresponds to the ratios of Cu and O in Cu_2O. Most analysis spots at the center of the CuNPs reveal a 90+% Cu content. To further verify that the nanoparticles do, in fact, have a Cu_2O shell and that there exists no bias from EDAX mapping, a separate set of EDAX analyses was conducted on Cu_2O nanocubes control where the Cu_2O phase should be evenly distributed throughout the nanoparticle. The results shown in Figure 4C,D reveal a uniform distribution of Cu and O content across these nanoparticles, which confirms that the Cu_2O is indeed intrinsic to the outermost shell of the CuNPs used in this study.

Depositing CuNPs on Ag films leads to the formation of an active Ag_2O−Cu_2O interface. C. Tseng reports significantly increased photocurrent measurements on Ag_2O−Cu_2O. Additionally, Guleria showed that Ag_2O−Cu_2O prepared via ultrasonic wet impregnation leads to significantly enhanced

https://doi.org/10.1021/acsomega.3c04303
ACS Omega 2023, 8, 34919−34927

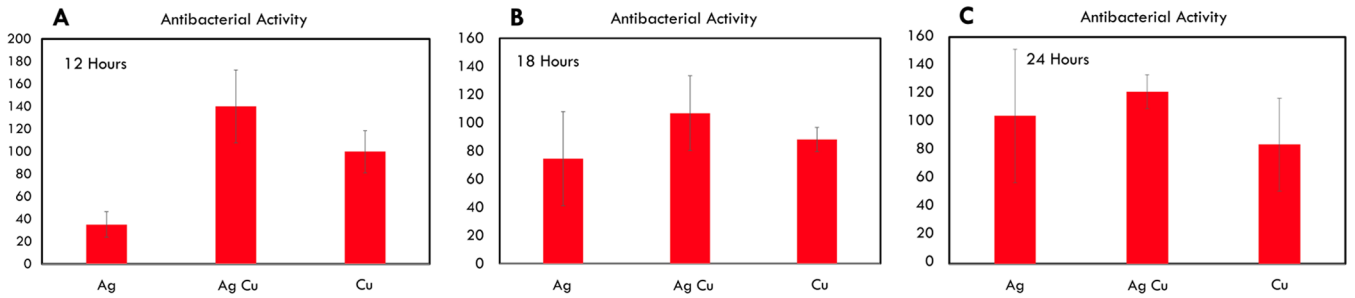

Figure 5. Results of antibacterial assessment for sample sets including Ag, Ag−Cu, and Cu samples at (A) 12 h, (B) 18 h, and (C) 24 h.

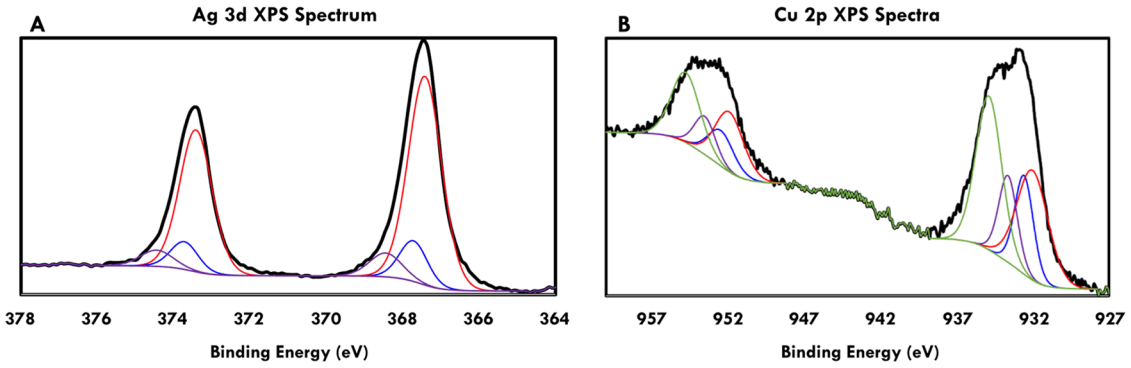

Figure 6. (A) Ag 3d HR-XPS spectra of Ag film in Ag−Cu samples. Features at 367.65, 367.95, and 368. 30 eV correspond to AgO, Ag_2O, and Ag, respectively. (B) HR-XPS spectrum of Cu 2p. Features at 932.0, 932.5, 933.59, and 934.88 eV correspond to Cu_2O, Cu metal, CuO, and $Cu(OH)_x$, respectively.

catalytic activity toward methylene blue dye degradation.[31] Ag_2O narrow band gap at 1.3 eV along with Cu_2O band gap of 2.0 eV, which sits in the infrared range, can lead to better charge separation processes at the material interfaces.[45,46] The synergy between these two interfacial contacts can lead to drastic changes in the antibacterial activity of the material and is the center of this investigation.

Antibacterial Assessment of Cu-on-Ag Planar Samples. Bacterial cell culture was cultivated in multiple well plates after CuNPs were drop-cast onto Ag thin film samples, and the cultures were then exposed to ambient light conditions. The OD values of the bacteria solutions were then measured and used for assessing the antibacterial efficiencies of the film samples based on the following equation

$$\%\frac{\text{microbial inhibition}}{\text{cm}^2} = \frac{\Delta\text{OD}}{\text{OD}_{\text{full,abs}} \times \text{area}} \times 100\% = \frac{(\text{OD}_{\text{full}} - \text{OD}_{\text{measured}})}{(\text{OD}_{\text{full}} - \text{OD}_{\text{null}}) \times \text{area}} \times 100\%$$

where OD_{full} denotes the value of the control well, representing the bacterial solution without any film samples, $OD_{measured}$ is the measured value of the well of interest, OD_{null} is the value of the blank control, which is the broth without bacteria, and area denotes the surface area of the film samples, expressed in cm^2 and calculated using ImageJ software.

Figure 5 illustrates the results of the antibacterial assessment on Ag−Cu samples at 6 h intervals, all measurements were conducted in triplicates to obtain error bars, and the activity of each sample is normalized to the planar surface area of each sample. Refer to Table S3 for the exact values of the measured OD from each sample. Figure 5A shows the antibacterial activity of CuNPs deposited on Si wafer, CuNPs deposited on Ag thin films, and bare Ag thin film samples at 12 h. It is clear that the presence of Ag−Cu leads to significant enhancement in the antibacterial activity of the sample, whereas the activity of bare Ag films and CuNPs controls are both lower than Ag−Cu samples. Figure S7 in the Supporting Information shows SEM analysis of *E. coli* on Ag−Cu and bare Ag surfaces. Ag−Cu shows a significant increase in *E. coli* death relative to bare Ag. XPS atomic fraction analysis reveals a surface coverage comprising 45% CuNPs, in which both copper and silver phases are reasonably exposed. Figure 5B shows results collected at 18 h, and Figure 5C at 24 h, respectively. The effect of the Ag−Cu interface remains observable even at 24 h. The activity of Ag is relatively higher at longer time durations (18 and 24 h) because the Ag film becomes unstable at longer time intervals. This instability was visually evidenced by areas of missing Ag films on the sample. This can result in additional Ag being released from the bulk into the bacterial medium. Given that Ag films were deposited via electron-beam deposition at 100 nm, deterioration of these films could expose the underlying bulk Ag to the bacterial medium. Ag−Cu however remains as the sample with the highest activity. While it is clear that the synergistic effect between Ag_2O−Cu_2O heterostructure exists, a mechanistic picture of how these two metal phases can induce such potent antibacterial activity has not yet been fully established. Thus, further spectroscopic analysis is required to elucidate the origins of these effects.

XPS Analysis of Ag−Cu and Proposed Mechanism. To fully understand the observed enhancement, we performed XPS analysis on Ag−Cu samples, as shown in Figure 6. Figure 6A displays the Ag 3d spectra of the Ag−Cu sample, with

https://doi.org/10.1021/acsomega.3c04303
ACS Omega 2023, 8, 34919−34927

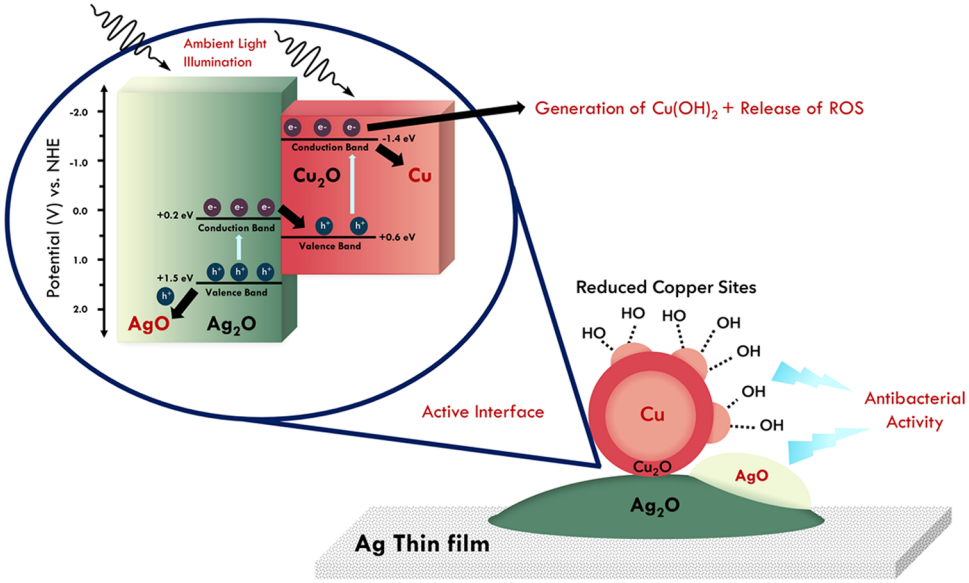

Figure 7. Proposed mechanism scheme demonstrating how the Ag−Cu interface mediates the enhanced antibacterial activity.

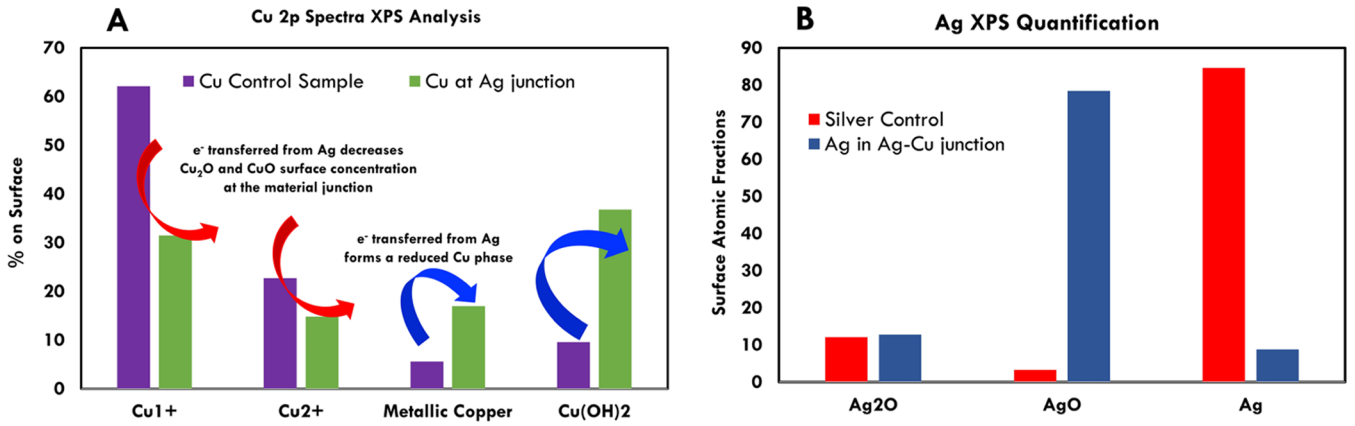

Figure 8. Detailed information about the relative concentrations of all surface species at active Ag−Cu samples. (A) Transfer of electrons across the different copper phases. Cu_2O remains the primary Cu phase; however, both Cu_2O and CuO are markedly reduced due to electrons transferred from silver. The presence of metallic copper is enhanced 2-fold, and a pronounced $Cu(OH)_x$ phase is observed. (B) Ag_2O remains stable both pre- and post-deposition of Cu nanoparticles on Ag surfaces. Metallic silver is dramatically oxidized to Ag^{2+}, as shown above.

binding energies of 367.65, 367.95, and 368.30 eV corresponding to AgO, Ag_2O, and Ag, respectively.[43] It is clear that upon the deposition of CuNPs on Ag, metallic Ag dramatically decreases. Figure 6B depicts Cu 2p XPS spectra with features at 932.0, 932.5, 933.59, and 934.88 eV, which correspond to Cu_2O, Cu, CuO, and $Cu(OH)_2$ phases.[43] The oxidization of Ag is followed by a dramatic increase in metallic Cu and a significant rise in the $Cu(OH)_2$ phase. Oxidation of Ag, evident in the large fraction of Ag^{2+} present on the surface and the reduction of Cu, is indicative of a charge transfer process between the Cu and Ag phases upon the formation of Ag−Cu interface sites. The most pronounced alteration in the Cu phase is the emergence of an increased $Cu(OH)_2$ phase at 934.88 eV. The observed phases upon the formation of Ag−Cu interfaces can be directly correlated to the observed antibacterial activity, which arises when Ag and Cu are placed in close proximity.

The formation of interface sites between Cu_2O (VB +0.6 eV, CB −1.4 eV, band gap 2.0 eV) and Ag_2O (VB +1.5 eV, CB +0.2 eV, band gap 1.3 eV) has been implicated in leading to enhanced photoinduced charge separation via a direct Z-scheme mechanism.[45,46] At close interfacial contact, band bending occurs, allowing for charge carrier recombination to take place between the two oxides.[7] Figure 7 depicts a proposed mechanism scheme that represents the different phases involved in the antibacterial process on Ag−Cu film samples.

As seen in Figure 7, under visible light illumination, electrons are excited from the valence band of Ag_2O to the conduction band and recombine with photogenerated holes in the valence band of Cu_2O. Over time, excited electrons build up on the copper surface, rendering the surface of Cu reduced, as evidenced by XPS analysis, while electrons in the conduction band of Cu_2O can also induce the formation of ROS, such as O_2^-, and $OH^\bullet$, which has been reported to form on similar systems.[31,47−49] Consequently, the formation of ROS species might also lead to $Cu(OH)_2$ as hydrogen abstraction from other oxygen-based surface species may occur to help yield the antibacterial.O_2^-, $OH^\bullet$, and other reactive species. Holes that build up on the surface of Ag can render the surface of Ag film more oxidized forming the antibacterial phase AgO, as shown in XPS analysis. The formation of

https://doi.org/10.1021/acsomega.3c04303
ACS Omega 2023, 8, 34919−34927

$Cu(OH)_2$ is quite significant since several reports have indicated that the formation of $Cu(OH)_2$ is directly related to enhanced release of ROS as well as increased amounts of Cu ions, as shown in previous studies, to exhibit the antibacterial effects by disrupting ATP production and impairing bacterial cell wall.[8,9,16,19,20] The formation of AgO is also significant as AgO has been reported to exhibit superior antibacterial activity relative to other Ag phases.[50]

To further confirm the production of ROS species, we performed methylene blue degradation experiments on both bare Ag and Ag−Cu samples. MB degradation occurs when ROS species form at the valence band and conduction band of the material. These species then react directly with the dye molecules; for more information, refer to Scheme 1 in the Supporting Information. A faster decrease in absorption signifies the formation of ROS species, which react with the MB dye resulting in dye degradation. Figure S6 in the Supporting Information reveals faster decay rates for Ag−Cu versus bare Ag, indicating enhanced formation of ROS species at the material interface.

To further substantiate the important role of the interface between the two materials, additional experiments were conducted on an inverse surface system where the coverage of Ag nanocubes was controlled on thermally evaporated Cu films using Langmuir−Blodgett deposition (LB); the procedure for sample fabrication is provided in the Supporting Information. TEM images of Ag nanocubes are shown in Figure S3, and SEM images of various coverages of Ag nanocube samples on Cu films are shown in Figure S4. The antibacterial activity of these samples was assessed, with results revealing the highest activity in samples where the dispersion of Ag nanocubes was maximized and good interfacial contact can be established between the Ag nanocubes and the Cu surface as shown in Figure S5.

Figure 8 presents the XPS quantification of the phases involved in this process. From Figure 8B, the surface concentration of Ag_2O remains largely unchanged between bare Ag films and Ag in Ag−Cu samples, indicating the high stability of the Ag_2O phase. This phase is important as its presence on the surface of the support film allows for the formation of a heterostructure with Cu_2O. Following the previously proposed Z-scheme mechanism, electrons from the conduction band of Ag_2O and holes from the Cu_2O's valence band recombine at the interface of the two materials. This is followed by the buildup of surface holes on Ag, consequently leading to an increase in AgO (Ag^{2+}) by over 14-fold. Dellasega et al. have reported that AgO exhibits remarkable antibacterial activity, which contributes to the Ag−Cu synergistic antibacterial enhancement.[50] Electrons that build up on the CuNPs are injected into the Cu_2O shell of the CuNPs, leading to a decrease in the surface concentration of Cu_2O (Cu^{1+}) by 2-fold as seen in Figure 8A. Despite this decrease, Cu_2O still remains a major proponent of the nanoparticle surface as its percent surface coverage still accounts for up to 30% of the nanoparticle surface. As expected, the surface concentration of CuO (Cu^{2+}) also experiences a decrease by 2-fold. The decrease in both Cu_2O and CuO results in a 3- to 4-fold increase in metallic Cu and $Cu(OH)_2$. We hypothesize that electrons transferred to the Cu nanoparticles are responsible for forming metallic Cu sites and $Cu(OH)_2$ via the previously proposed Z-scheme mechanism. Both of these phases have been reported to be able to contribute substantially to the intrinsic antibacterial activity of the material by inducing the release of Cu ions and ROS species. In addition, the highly oxidized AgO phase also contributes substantially to the antibacterial activity of the material. The correlation of these active phases involved, as well as the activity correlation with the Ag−Cu interface, provides strong insights into the origins of the antibacterial activity in a bifunctional surface system, which is otherwise not yet fully explored.

CONCLUSIONS

We investigated in this study the enhanced antibacterial activity induced by the contact of two metals: copper and silver. Colloidal CuNPs were synthesized, deposited on silver thin films, and investigated for antibacterial activity against *Escherichia coli*. TEM and EDAX analyses indicate that CuNPs are enclosed in a Cu_2O shell. XPS measurements demonstrate that depositing CuNPs on Ag films forms a photoactive Cu_2O−Ag_2O heterostructure. A Z-scheme mechanism was proposed to explain Ag−Cu's bifunctionality. First, electrons in the Ag_2O conduction band recombine with holes in the Cu_2O valence band. Electrons from the conduction band of Cu_2O can be transferred to nearby $Cu^{1+/2+}$ sites, thereby rendering a reduced Cu surface. Simultaneously, these electrons can also be transferred to surface oxygen species, leading to the formation of ROS and $Cu(OH)_2$. Cu and $Cu(OH)_2$ have previously been proposed in the literature as active antibacterial phases and have been directly correlated to the release of ROS species and Cu ions. The buildup of holes on Ag_2O's valence band leads to the oxidation of Ag, resulting in the production of the highly antibacterial AgO phase. Quantitative analysis of HR-XPS spectra reveals an upsurge in the $Cu(OH)_2$ phase by 4-fold and AgO by 14-fold. For the first time, this study provides strong evidence that the antibacterial activity of simple Ag−Cu systems may originate from a Z-scheme charge transfer process occurring at the interface of the Cu_2O and Ag_2O phases present on both Ag and Cu surfaces. Prior to this study, several reports have shown increased antibacterial activity when Ag and Cu are utilized together as antibacterial materials. The results of this study are insightful as they address the mechanistic question of the origins of the antibacterial activity observed in simple Ag−Cu colloid thin film systems.

ASSOCIATED CONTENT

Supporting Information

The Supporting Information is available free of charge at https://pubs.acs.org/doi/10.1021/acsomega.3c04303.

TEM images of Cu nanoparticles and Ag nanocubes; data tables for antibacterial activity calculations and image analyses; antibacterial activities of Ag Nanocubes on Cu films; accompanying SEM images of Ag nanocube coverages on Cu film; methylene blue degradation rates for Ag−Cu and Cu samples; SEM images of *E. coli* on samples; and methods for Cu thin film deposition and Ag nanocube synthesis (PDF)

AUTHOR INFORMATION

Corresponding Authors

Sakol Warintaraporn − *Department of Chemistry, Kamnoetvidya Science Academy, Rayong 21210, Thailand*; Email: Sakol.w@kvis.ac.th

https://doi.org/10.1021/acsomega.3c04303
ACS Omega 2023, 8, 34919−34927

Yutichai Mueanngern − *Department of Chemistry, Kamnoetvidya Science Academy, Rayong 21210, Thailand;* orcid.org/0000-0002-0618-9989; Email: yutichai.m@kvis.ac.th

Authors

Weerapat Li − *Department of Chemistry, Kamnoetvidya Science Academy, Rayong 21210, Thailand*

Supphanat Anantachaisophon − *Department of Chemistry, Kamnoetvidya Science Academy, Rayong 21210, Thailand*

Thanakrit Vachiraanun − *Department of Chemistry, Kamnoetvidya Science Academy, Rayong 21210, Thailand*

Worachon Promchaisri − *Department of Chemistry, Kamnoetvidya Science Academy, Rayong 21210, Thailand*

Pongpop Sangsawang − *Department of Chemistry, Kamnoetvidya Science Academy, Rayong 21210, Thailand*

Pattarapon Tanalikhit − *Department of Physics, Korea Advanced Institute of Science and Technology, Daejeon 34141, Republic of Korea;* orcid.org/0000-0002-4809-6668

Somlak Ittisanronnachai − *Frontier Research Center (FRC), Vidyasirimedhi Institute of Science and Technology, Rayong 21210, Thailand*

Thassanant Atithep − *Frontier Research Center (FRC), Vidyasirimedhi Institute of Science and Technology, Rayong 21210, Thailand*

Passapan Sanguanchua − *Department of Chemistry, Kamnoetvidya Science Academy, Rayong 21210, Thailand*

Arjaree Ratanasangsathien − *Department of Chemistry, Kamnoetvidya Science Academy, Rayong 21210, Thailand*

Mathus Jirapunyawong − *Department of Chemistry, Kamnoetvidya Science Academy, Rayong 21210, Thailand*

Siriporn Suntiworapong − *Department of Biology, Kamnoetvidya Science Academy, Rayong 21210, Thailand*

Complete contact information is available at: https://pubs.acs.org/10.1021/acsomega.3c04303

Author Contributions

[⊥]W.L., S.A., T.V., W.P., and P.S. contributed equally to this work.

Notes

The authors declare no competing financial interest.

■ ACKNOWLEDGMENTS

This work was fully funded by Kamnoetvidya Science Academy. Sample characterization was performed at Vidyasirimedhi Institute of Science and Technology. The authors also thank Dr. Taweesak Sudyodsuk at Vidyasirimedhi Institute of Science and Technology for assisting in the preparation of thermal evaporated thin film samples.

■ REFERENCES

(1) Linklater, D. P.; Ivanova, E. P. Nanostructured Antibacterial Surfaces − What Can Be Achieved? *Nano Today* **2022**, *43*, No. 101404.

(2) Balasubramaniam, B.; Prateek; Ranjan, S.; Saraf, M.; Kar, P.; Singh, S. P.; Thakur, V. K.; Singh, A.; Gupta, R. K. Antibacterial and Antiviral Functional Materials: Chemistry and Biological Activity toward Tackling COVID-19-like Pandemics. *ACS Pharmacol. Transl. Sci.* **2021**, *4*, 8−54.

(3) Ren, Y.; Liu, H.; Liu, X.; Zheng, Y.; Li, Z.; Li, C.; Yeung, K. W. K.; Zhu, S.; Liang, Y.; Cui, Z.; Wu, S. Photoresponsive Materials for Antibacterial Applications. *Cell Rep. Phys. Sci.* **2020**, *1*, No. 100245.

(4) Su, C.; Ye, Y.; Qiu, H.; Zhu, Y. Solvent-Free Fabrication of Self-Regenerating Antibacterial Surfaces Resisting Biofilm Formation. *ACS Appl. Mater. Interfaces* **2021**, *13*, 10553−10563.

(5) Siegel, J.; Kolářová, K.; Vosmanská, V.; Rimpelová, S.; Leitner, J.; Švorčík, V. Antibacterial Properties of Green-Synthesized Noble Metal Nanoparticles. *Mater. Lett.* **2013**, *113*, 59−62.

(6) Slavin, Y. N.; Asnis, J.; Häfeli, U. O.; Bach, H. Metal Nanoparticles: Understanding the Mechanisms behind Antibacterial Activity. *J. Nanobiotechnol.* **2017**, *15*, No. 65.

(7) Yuan, Y.; Guo, R.-t.; Hong, L.-f.; Ji, X.-y.; Lin, Z.-d.; Li, Z.-s.; Pan, W.-g. A Review of Metal Oxide-Based Z-Scheme Heterojunction Photocatalysts: Actualities and Developments. *Mater. Today Energy* **2021**, *21*, No. 100829.

(8) Ben-Sasson, M.; Zodrow, K. R.; Genggeng, Q.; Kang, Y.; Giannelis, E. P.; Elimelech, M. Surface Functionalization of Thin-Film Composite Membranes with Copper Nanoparticles for Antimicrobial Surface Properties. *Environ. Sci. Technol.* **2014**, *48*, 384−393.

(9) Grass, G.; Rensing, C.; Solioz, M. Metallic Copper as an Antimicrobial Surface. *Appl. Environ. Microbiol.* **2011**, *77*, 1541−1547.

(10) Bruna, T.; Maldonado-Bravo, F.; Jara, P.; Caro, N. Silver Nanoparticles and Their Antibacterial Applications. *Int. J. Mol. Sci.* **2021**, *22*, No. 7202.

(11) Shrestha, A.; Kishen, A. Antibacterial Nanoparticles in Endodontics: A Review. *J. Endod.* **2016**, *42*, 1417−1426.

(12) Xu, V. W.; Nizami, M. Z. I.; Yin, I. X.; Yu, O. Y.; Lung, C. Y. K.; Chu, C. H. Application of Copper Nanoparticles in Dentistry. *Nanomaterials* **2022**, *12*, No. 805.

(13) Ingle, A. P.; Duran, N.; Rai, M. Bioactivity, Mechanism of Action, and Cytotoxicity of Copper-Based Nanoparticles: A Review. *Appl. Microbiol. Biotechnol.* **2014**, *98*, 1001−1009.

(14) Shah, K. N.; Shah, P. N.; Mullen, A. R.; Chen, Q.; Southerland, M. R.; Chirra, B.; DeBerardinis, R. J.; Cannon, C. L. N-Acetyl Cysteine Abrogates Silver-Induced Reactive Oxygen Species in Human Cells without Altering Silver-Based Antimicrobial Activity. *Toxicol. Lett.* **2020**, *332*, 118−129.

(15) Steward, M. R. *The Role of Redox Chemistry of Disulfide Bonds in Cysteine Residues of Membrane Proteins by Cuprous and Cupric Ions in Cell Death of E. coli*; Portland State University, 2020.

(16) Chatterjee, A. K.; Chakraborty, R.; Basu, T. Mechanism of Antibacterial Activity of Copper Nanoparticles. *Nanotechnology* **2014**, *25*, No. 135101.

(17) Feng, Q. L.; Wu, J.; Chen, G. Q.; Cui, F. Z.; Kim, T. N.; Kim, J. O. A Mechanistic Study of the Antibacterial Effect of Silver Ions on Escherichia coli and Staphylococcus Aureus. *J. Biomed. Mater. Res.* **2000**, *52*, 662−668.

(18) Nan, L.; Yang, W.; Liu, Y.; Yang, K. *Antibacterial Mechanism of Copper-Bearing Antibacterial Stainless Steel against E.coli*, 2008; Vol. *24*.

(19) Clavier, B.; Baptiste, T.; Zhadan, A.; Guiet, A.; Boucher, F.; Brezová, V.; Roques, C.; Corbel, G. Understanding the Bactericidal Mechanism of $Cu(OH)_2$ Nanorods in Water through Mg-Substitution: High Production of Toxic Hydroxyl Radicals by Non-Soluble Particles. *J. Mater. Chem. B* **2022**, *10*, 779−794.

(20) Karkhanechi, H.; Takagi, R.; Ohmukai, Y.; Matsuyama, H. Enhancing the Antibiofouling Performance of RO Membranes Using Cu(OH)2 as an Antibacterial Agent. *Desalination* **2013**, *325*, 40−47.

(21) Bankier, C.; Matharu, R. K.; Cheong, Y. K.; Ren, G. G.; Cloutman-Green, E.; Ciric, L. Synergistic Antibacterial Effects of Metallic Nanoparticle Combinations. *Sci. Rep.* **2019**, *9*, No. 16074.

(22) Zheng, N.; Stucky, G. D. A General Synthetic Strategy for Oxide-Supported Metal Nanoparticle Catalysts. *J. Am. Chem. Soc.* **2006**, *128*, 14278−14280.

(23) Bruix, A.; Rodriguez, J. A.; Ramírez, P. J.; Senanayake, S. D.; Evans, J.; Park, J. B.; Stacchiola, D.; Liu, P.; Hrbek, J.; Illas, F. A New Type of Strong Metal−Support Interaction and the Production of H_2 through the Transformation of Water on Pt/CeO_2 (111) and $Pt/CeO_x/TiO_2$ (110) Catalysts. *J. Am. Chem. Soc.* **2012**, *134*, 8968−8974.

(24) Perdikaki, A.; Galeou, A.; Pilatos, G.; Karatasios, I.; Kanellopoulos, N. K.; Prombona, A.; Karanikolos, G. N. Ag and Cu

Monometallic and Ag/Cu Bimetallic Nanoparticle-Graphene Composites with Enhanced Antibacterial Performance. *ACS Appl. Mater. Interfaces* **2016**, *8*, 27498−27510.
(25) Hans, M.; Támara, J. C.; Mathews, S.; Bax, B.; Hegetschweiler, A.; Kautenburger, R.; Solioz, M.; Mücklich, F. Laser Cladding of Stainless Steel with a Copper-Silver Alloy to Generate Surfaces of High Antimicrobial Activity. *Appl. Surf. Sci.* **2014**, *320*, 195−199.
(26) Egger, S.; Lehmann, R. P.; Height, M. J.; Loessner, M. J.; Schuppler, M. Antimicrobial Properties of a Novel Silver-Silica Nanocomposite Material. *Appl. Environ. Microbiol.* **2009**, *75*, 2973−2976.
(27) Mukha, I.; Eremenko, A.; Korchak, G.; Michienkova, A. Antibacterial Action and Physicochemical Properties of Stabilized Silver and Gold Nanostructures on the Surface of Disperse Silica. *J. Water Resour. Prot.* **2010**, *02*, 131−136.
(28) Jin, T.; He, Y. Antibacterial Activities of Magnesium Oxide (MgO) Nanoparticles against Foodborne Pathogens. *J. Nanopart. Res.* **2011**, *13*, 6877−6885.
(29) Li, J.; Cushing, S. K.; Bright, J.; Meng, F.; Senty, T. R.; Zheng, P.; Bristow, A. D.; Wu, N. Ag@Cu2O Core-Shell Nanoparticles as Visible-Light Plasmonic Photocatalysts. *ACS Catal.* **2013**, *3*, 47−51.
(30) Feng, H.; Wang, W.; Wang, W.; Zhang, M.; Wang, C.; Ma, C.; Li, W.; Chen, S. Charge Transfer Channels of Silver @ Cuprous Oxide Heterostructure Core-Shell Nanoparticles Strengthen High Photocatalytic Antibacterial Activity. *J. Colloid Interface Sci.* **2021**, *601*, 531−543.
(31) Guleria, A.; Sharma, R.; Singh, A.; Upadhyay, N. K.; Shandilya, P. Direct Dual-Z-Scheme PANI/Ag2O/Cu2O Heterojunction with Broad Absorption Range for Photocatalytic Degradation of Methylene Blue. *J. Water Process Eng.* **2021**, *43*, No. 102305.
(32) Yu, W.; Porosoff, M. D.; Chen, J. G. Review of Pt-Based Bimetallic Catalysis: From Model Surfaces to Supported Catalysts. *Chem. Rev.* **2012**, *112*, 5780−5817.
(33) Hosseinidoust, Z.; Van De Ven, T. G. M.; Tufenkji, N. Bacterial Capture Efficiency and Antimicrobial Activity of Phage-Functionalized Model Surfaces. *Langmuir* **2011**, *27*, 5472−5480.
(34) Yang, X.; Mueanngern, Y.; Baker, Q. A.; Baker, L. R. Crotonaldehyde Hydrogenation on Platinum-Titanium Oxide and Platinum-Cerium Oxide Catalysts: Selective CO Bond Hydrogen Requires Platinum Sites beyond the Oxide-Metal Interface. *Catal. Sci. Technol.* **2016**, *6*, 6824−6835.
(35) Aditya, T.; Pal, A.; Pal, T. Nitroarene Reduction: A Trusted Model Reaction to Test Nanoparticle Catalysts. *Chem. Commun.* **2015**, *51*, 9410−9431.
(36) Akita, T.; Kohyama, M.; Haruta, M. Electron Microscopy Study of Gold Nanoparticles Deposited on Transition Metal Oxides. *Acc. Chem. Res.* **2013**, *46*, 1773−1782.
(37) Mueanngern, Y.; Li, C.-H.; Spelic, M.; Graham, J.; Pimental, N.; Khalifa, Y.; Jinschek, J. R.; Baker, L. R. Deactivation-Free Ethanol Steam Reforming at Nickel-Tipped Carbon Filaments. *Phys. Chem. Chem. Phys.* **2021**, *23*, 11764−11773.
(38) Zhang, Y.; He, X.; Ouyang, J.; Yang, H. Palladium Nanoparticles Deposited on Silanized Halloysite Nanotubes: Synthesis, Characterization and Enhanced Catalytic Property. *Sci. Rep.* **2013**, *3*, No. 2948.
(39) Tang, H.; Wei, J.; Liu, F.; Qiao, B.; Pan, X.; Li, L.; Liu, J.; Wang, J.; Zhang, T. Strong Metal−Support Interactions between Gold Nanoparticles and Nonoxides. *J. Am. Chem. Soc.* **2016**, *138*, 56−59.
(40) Wang, Y.; Chen, P.; Liu, M. Synthesis of Well-Defined Copper Nanocubes by a One-Pot Solution Process. *Nanotechnology* **2006**, *17*, 6000−6006.
(41) Thoka, S.; Lee, A.-T.; Huang, M. H. Scalable Synthesis of Size-Tunable Small Cu_2O Nanocubes and Octahedra for Facet-Dependent Optical Characterization and Pseudomorphic Conversion to Cu Nanocrystals. *ACS Sustainable Chem. Eng.* **2019**, *7*, 10467−10476.
(42) Ionita, D.; Grecu, M.; Ungureanu, C.; Demetrescu, I. Antimicrobial Activity of the Surface Coatings on TiAlZr Implant Biomaterial. *J. Biosci. Bioeng.* **2011**, *112*, 630−634.
(43) Naumkin, A. V.; Kraut-Vass, A.; Gaarenstroom, S. W.; Powell, C. J. NIST Standard Reference Database 20, Version 4.1 (web version). https://srdata.nist.gov/xps/2012.
(44) Over, H.; Seitsonen, A. P. Oxidation of Metal Surfaces. *Science* **2002**, *297*, 2003−2005.
(45) Deng, Y.; Tang, L.; Zeng, G.; Feng, C.; Dong, H.; Wang, J.; Feng, H.; Liu, Y.; Zhou, Y.; Pang, Y. Plasmonic Resonance Excited Dual Z-Scheme BiVO4/Ag/Cu2O Nanocomposite: Synthesis and Mechanism for Enhanced Photocatalytic Performance in Recalcitrant Antibiotic Degradation. *Environ. Sci. Nano* **2017**, *4*, 1494−1511.
(46) Zhou, L.; Zou, G.; Deng, H. The Roles of Graphene and Ag in the Hybrid Ag@Ag2O-Graphene for Sulfamethoxazole Degradation. *Catalysts* **2018**, *8*, No. 272.
(47) Liang, T. Y.; Chan, S. J.; Patra, A. S.; Hsieh, P. L.; Chen, Y. A.; Ma, H. H.; Huang, M. H. Inactive Cu2O Cubes Become Highly Photocatalytically Active with Ag2S Deposition. *ACS Appl. Mater. Interfaces* **2021**, *13*, 11515−11523.
(48) Liu, Y.; Zeng, X.; Easton, C. D.; Li, Q.; Xia, Y.; Yin, Y.; Hu, X.; Hu, J.; Xia, D.; McCarthy, D. T.; Deletic, A.; Sun, C.; Yu, J.; Zhang, X. An: In Situ Assembled WO3-TiO2 Vertical Heterojunction for Enhanced Z-Scheme Photocatalytic Activity. *Nanoscale* **2020**, *12*, 8775−8784.
(49) Ibrahim, M. M.; Mezni, A.; El-Sheshtawy, H. S.; Zaid, A. A. A.; Alsawat, M.; El-Shafi, N.; Ahmed, S. I.; Shaltout, A. A.; Amin, M. A.; Kumeria, T.; Altalhi, T. Direct Z-Scheme of Cu 2 O/TiO 2 Enhanced Self-Cleaning, Antibacterial Activity, and UV Protection of Cotton Fiber under Sunlight. *Appl. Surf. Sci.* **2019**, *479*, 953−962.
(50) Dellasega, D.; Facibeni, A.; Di Fonzo, F.; Bogana, M.; Polissi, A.; Conti, C.; Ducati, C.; Casari, C. S.; Bassi, A. L.; Bottani, C. E. Nanostructured Ag4O4 Films with Enhanced Antibacterial Activity. *Nanotechnology* **2008**, *19*, No. 475602.

https://doi.org/10.1021/acsomega.3c04303
ACS Omega 2023, 8, 34919−34927